Inorganic Chemistry
Cite This: Inorg. Chem. 2019, 58, 7785−7793
Article
pubs.acs.org/IC

# Evidence for Reagent-Induced Spin-State Switching in Tripodal Fe(II) Iminopyridine Complexes

Tarik J. Ozumerzifon,[†,#] Robert F. Higgins,[†,∥] Justin P. Joyce,[†] Jacek L. Kolanowski,[⊥] Anthony K. Rappé,[†] and Matthew P. Shores*[,†]

[†]Department of Chemistry, Colorado State University, Fort Collins, Colorado 80523, United States
[⊥]Institute of Bioorganic Chemistry, Polish Academy of Sciences, Noskowskiego 12/14, 61-704 Poznań, Poland

Supporting Information

**ABSTRACT:** We present evidence of a spin-state change that accompanies desilylation reactions performed on two related Fe(II) iminopyridine coordination complexes. To probe these systems, we performed titrations with CsF in solution and analyzed the speciation with in situ magnetometry, electrochemistry, and mass spectrometry techniques. We find that pendant *tert*-butyldimethylsilyl groups are readily cleaved under these conditions, and the resulting desilylated complexes exhibit overall decreased solution magnetic susceptibility values. Density functional theory and *ab initio* computations probe the impact of substituent identity (prior to- and post-desilylation) on the metal−ligand $\sigma$-donor and $\pi$-acceptor bonding properties. We attribute the observed spin-state changes to the decrease in entropy associated with the conformational freedom of the silylated high-spin complex, resulting in a more favored low-spin state upon desilylation.

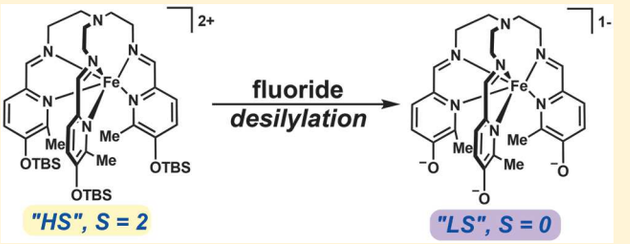


## INTRODUCTION

Spin crossover (SCO) enables molecular switching functions due to dramatic contrasts in magnetic, structural, and spectroscopic properties between spin-states. The low- to high-spin (LS and HS, respectively) conversion involves a weakening of the ligand field ($\Delta H > 0$) that is compensated by an increasing number of electronic microstates and lower-energy vibrational modes ($\Delta S > 0$). This molecular phenomenon has been controlled through external perturbations such as temperature, pressure, and light.[1−7]

Ligand substituents play a complicated role in determining SCO properties. For example, steric bulk can perturb equilibrium metal−ligand bond lengths in both molecules and soft materials,[8−15] while hydrogen-bonding interactions have also been shown to affect ligand donor properties.[16,17] Recent reports describe linear relationships between solution-phase SCO temperatures ($T_{1/2} = \Delta H/\Delta S$) and electronic character of the substituents for Fe(II) complexes.[18−22] These trends are often system-dependent due to competing impacts on the ligand field strength via $\sigma$-donor and $\pi^*$-acceptor interactions.

Postsynthetic modification of a ligand scaffold offers an attractive approach to affect changes to spin-state properties, with potential to inspire new motifs for environmental sensing, imaging, and memory devices.[23−25] Several groups have reported reagent-induced spin-state changes through chemical transformations of the coordinated ligand set.[26−33] We are motivated by the work of Hooley and Nitschke, who have shown that the distinct reactivity of coordinated iminopyridine ligands in Fe(II) cage complexes provides a direct synthetic route for the alteration of functional groups.[34−38]

We chose to explore the feasibility of *chemical* modulation of the spin-state in an Fe(II) iminopyridine podand to generate design principles for future sensing architectures. Building on our and others' experience with manipulating spin states in metal iminopyridine complexes, a model synthetic target is depicted in Figure 1.[8−10,39,40]

We envision that cleavage of a fluoride-sensitive silyl ether moiety will impart a significant change in ligand field, given the large differences in Hammett parameters ($\sigma_{meta}$ and $\sigma_{para}$) for the reactant (silyl ether) and product ("phenoxide") substituents. Of course, the protonation state of the desilylated products will depend on reaction conditions, ultimately affecting the electronic nature of that 5-pyridyl substituent. In our proposed system, Fe(II) complexes with two different tripodal ligands will allow us to evaluate the impact of electronic and other factors on low- and high-spin species. The spectroscopic, mass spectrometric, electrochemical, and magnetic data presented herein shed light on the complex dynamics of these desilylation reactions. Computations probe fluctuations in ligand $\sigma$- and $\pi$-bonding properties, to deconvolute the electronic impacts of substituent changes on the bidentate iminopyridine ligand set that places the 5-pyridyl substituents *-meta* and *-para* to the pyridine and imine nitrogen atoms, respectively.

**Received:** February 5, 2019
**Published:** May 28, 2019






DOI: 10.1021/acs.inorgchem.9b00340
Inorg. Chem. 2019, 58, 7785−7793

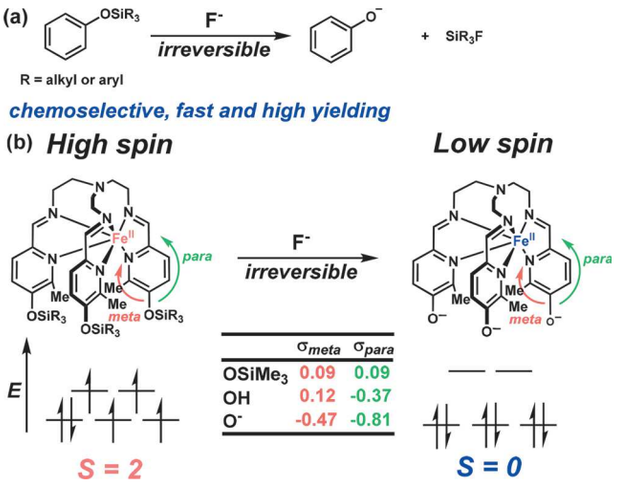


**Figure 1.** (a, b) Proposed method for spin-state changing in Fe(II) podand complexes.[41] While the expected formation of phenoxide species is depicted, the actual protonation state of the desilylated products may depend on reaction conditions.

## EXPERIMENTAL SECTION

Note: No unexpected or significant safety hazards occurred in the present work. The use of perchlorate salts is mentioned in more detail later (vide infra).

**Preparation of Compounds.** Unless otherwise stated, reactions were performed under ambient conditions (room temperature, normal benchtop atmosphere). Air-free manipulations were carried out in a dinitrogen-filled glovebox (MBRAUN Labmaster 130). Qualitative thin layer chromatography (TLC) analysis was performed on 250 mm thick, 60 Å, glass backed, F254 silica (Silicycle, Quebec City, Canada); samples were visualized with UV light. Flash chromatography was performed using Silicycle silica gel (230−400 mesh). Syringe filters were purchased from VWR International and were fitted with 0.2 $\mu$m PTFE membranes. Diethyl ether ($Et_2O$), dichloromethane ($CH_2Cl_2$), and acetonitrile (MeCN) were sparged with nitrogen, passed through alumina columns, and degassed prior to use. Anhydrous ethanol (EtOH) and methanol (MeOH) were purchased from Sigma-Aldrich. All other chemicals were purchased from commercial vendors and used as received.

*5-(tert-Butyldimethylsilyloxy)picolinaldehyde (**1**).* Crude 5-hydroxypicolinaldehyde (**1A**,[9] see Supporting Information for preparation), *tert*-butyldimethylchlorosilane (TBSCl, 3.00 g, 19.9 mmol), and *N*,*N*-dimethylaminopyridine (DMAP, 0.220 g, 1.8 mmol) were charged to a flame-dried flask and then dissolved in $CH_2Cl_2$ (36 mL) and cooled to 0 °C. Then, freshly distilled triethylamine (3.03 mL, 21.7 mmol) was added dropwise, and the resulting mixture was warmed to 23 °C and stirred for 1 h. The reaction mixture was then quenched with water and poured into a separatory funnel; the crude product was extracted with $CH_2Cl_2$ (2 × 20 mL), washed with brine (20 mL), dried over $MgSO_4$, and filtered. The desired compound was purified by flash column chromatography (4:1 hexanes/EtOAc eluent) to give pure silyl ether **1** (1.93 g, 87% yield over two steps; see Supporting Information for previous step), as a pale yellow oil. $R_f$ = 0.65 in 4:1 hexanes/EtOAc. $^1$H NMR (400 MHz, $CDCl_3$): $\delta$ 9.99 (s, 1H), 8.34 (d, $J$ = 2.3 Hz, 1H), 7.91 (d, $J$ = 8.6 Hz, 1H), 7.25 (app. dd, $J$ = 2.3 Hz, 1H), 1.00 (s, 9H), 0.28 (s, 6H). $^{13}$C NMR (100 MHz, $CDCl_3$): $\delta$ 192.0, 156.1, 146.7, 142.9, 126.8, 123.2, 25.5, 18.2, −4.4. IR (ATR, film): 2956, 2931, 2859, 1710, 1574, 1478, 1391, 1363, 1292, 1257, 1210, 1111, 1013 cm$^{-1}$. HRMS (ESI$^+$): $m/z$ calcd for (M + H)$^+$ [$C_{12}H_{20}NO_2Si$ + H]$^+$: 238.1263, found: 238.1242.

*[Fe(5-OTBSpy)$_3$ tren](OTf)$_2$ (**2**).* In a dinitrogen glovebox, to a solution of **1** (0.200 g, 0.84 mmol) in MeCN (2 mL) was added a solution of tris(2-aminoethyl)amine (tren, 0.040 g, 0.27 mmol) in MeCN (2 mL), and the resulting mixture was stirred in the presence of 3 Å molecular sieves for 1 h at 23 °C. Then, a solution of $Fe(OTf)_2(MeCN)_2$ (0.119 g, 0.27 mmol) in MeCN (2 mL) was added dropwise, and the resulting dark red mixture was stirred for an additional 1 h at 23 °C. The reaction mixture was then passed through a syringe filter, and the product was precipitated by addition of $Et_2O$ (20 mL) to the filtrate. The mixture was stirred overnight, and the solid was collected by filtration and washed with $Et_2O$ (2 × 5 mL) to afford **2** (0.215 g, 68% yield) as a dark red powder. IR (KBr pellet): $\nu_{C=N}$ 1591 cm$^{-1}$. Absorption spectrum (acetone, $Me_2CO$): $\lambda_{max}$ ($\varepsilon_M$) 354 nm (25 900 M$^{-1}$ cm$^{-1}$), 553 nm (7770 M$^{-1}$ cm$^{-1}$). MS (ESI$^+$): $m/z$ calcd for (M − OTf)$^+$ [$C_{44}H_{69}N_7O_9Si_3S_2F_6Fe$ − $CF_3SO_3$]$^+$: 1008.36, found: 1008.33; $m/z$ calcd for (M − 2OTf)$^{2+}$ [$C_{44}H_{69}N_7O_9Si_3S_2F_6Fe$ − $C_2F_6S_2O_6$]$^{2+}$: 429.71, found: 429.83. $^1$H NMR spectra are collected in Figure S39. $\chi_M T$ (298 K, $(CD_3)_2CO$): 0.17 cm$^3$ K mol$^{-1}$; Anal. Calcd for $C_{47}H_{73.5}N_{8.5}O_9Si_3S_2F_6Fe$ (**2**·1.5MeCN): C, 46.28; H, 6.07; N, 9.76. Found: C, 45.83; H, 5.65; N, 10.09. Note: samples prepared for elemental analysis were crystals grown from a layering of **2** in acetonitrile (3 mL) with a 1:1 antisolvent layer of $Et_2O$:$i$Pr$_2$O. Small quantities of diffraction-quality crystals can be grown by diffusion of $i$Pr$_2$O into a concentrated solution of **2** in acetonitrile; these do not contain co-crystallized MeCN solvent molecules.

*6-Methyl-5-(tert-butyldimethylsilyloxy)picolinaldehyde (**3**).* Crude 5-hydroxy-6-methyl-picolinaldehyde (**3A**,[9] see Supporting Information for preparation), TBSCl (2.22 g, 14.7 mmol), and DMAP (0.160 g, 1.33 mmol) were charged to a flame-dried flask and then dissolved in $CH_2Cl_2$ (27 mL) and cooled to 0 °C. Then, freshly distilled triethylamine (2.24 mL, 16.1 mmol) was added dropwise, and the resulting mixture was warmed to 23 °C and stirred for 1 h. The reaction mixture was then quenched with water and poured into a separatory funnel; the product was extracted with $CH_2Cl_2$ (2 × 20 mL), washed with brine (20 mL), dried over $MgSO_4$, and filtered to give crude **3**. The desired compound was purified by flash column chromatography (4:1 hexanes/EtOAc eluent) to give pure silyl ether **3** (2.13 g, 18% yield over three steps; see Supporting Information for previous two steps), as a pale yellow oil. $R_f$ = 0.67 in 4:1 hexanes/EtOAc). $^1$H NMR (400 MHz, $CDCl_3$): $\delta$ 9.95 (s, 1H), 7.76 (d, $J$ = 8.2 Hz, 1H), 7.12 (d, $J$ = 8.2 Hz, 1H), 2.53 (s, 3H), 1.03 (s, 9H), 0.28 (s, 6H). $^{13}$C NMR (100 MHz, $CDCl_3$): $\delta$ 192.3, 154.2, 152.0, 145.5, 124.3, 121.4, 25.5, 19.8, 18.2, −4.3. IR (ATR, film): 2956, 2931, 2859, 1702, 1566, 1456, 1347, 1303, 1278, 1257, 1245, 1170, 1112 cm$^{-1}$. HRMS (ESI$^+$): $m/z$ calcd for (M + H)$^+$ [$C_{13}H_{22}NO_2Si$ + H]$^+$: 252.1420, found: 252.1391.

*[Fe(6-Me-5-OTBSpy)$_3$tren](ClO$_4$)$_2$ (**4**).* Caution! Although we have not encountered any difficulties with this product, perchlorate-containing compounds pose explosion hazards and should be handled with care and in small quantities.

In a dinitrogen glovebox, to a solution of **3** (0.100 g, 0.40 mmol) in MeCN (2 mL) was added a solution of tren (0.019 g, 0.13 mmol) in MeCN (2 mL), and the resulting mixture was stirred in the presence of 3 Å molecular sieves for 1 h at 23 °C. Then, a solution of $Fe(ClO_4)_2(H_2O)_{12}$ (0.060 g, 0.13 mmol) in MeCN (2 mL) was added dropwise, and the resulting red mixture was stirred for an additional 1 h at 23 °C. The reaction mixture was then passed through a syringe filter, and the product was precipitated by addition of $Et_2O$ (20 mL) to the filtrate. The mixture was stirred overnight. The crude product was recrystallized by placing a concentrated solution of **4** in EtOH into a freezer (−40 °C) overnight, giving pure **4** (0.109 g, 77% yield) as red needle-like crystals that are too brittle for analysis via single crystal X-ray diffraction. IR (KBr pellet): $\nu_{C=N}$ 1653 cm$^{-1}$. Absorption spectrum ($Me_2CO$): $\lambda_{max}$ ($\varepsilon_M$) 437 nm (3920 M$^{-1}$ cm$^{-1}$). MS (ESI$^+$) $m/z$ calcd for (M - $ClO_4$)$^+$ [$C_{45}H_{75}N_7O_{11}Cl_2Si_3Fe$ − $ClO_4$]$^+$: 1000.41, found 1000.42, $m/z$ calcd for (M − 2$ClO_4$)$^{2+}$ [$C_{45}H_{75}N_7O_{11}Cl_2Si_3Fe$ − $Cl_2O_8$]$^{2+}$: 450.73, found 450.75. $^1$H NMR spectra are collected in Figure S40. $\chi_M T$ (298 K, $(CD_3)_2CO$): 3.44 cm$^3$ K mol$^{-1}$. $\chi_M T$ (300 K, solid state): 3.89 cm$^3$ K mol$^{-1}$. Anal. Calcd for $C_{45}H_{75}N_7O_{11}Cl_2Si_3Fe$: C, 49.09; H, 6.87; N, 8.90. Found: C, 48.94; H, 6.75; N, 8.97.

**Physical Methods.** All methods were performed at room temperature unless otherwise noted. Absorption spectra were obtained with a Hewlett-Packard 8453 spectrometer in quartz


DOI: 10.1021/acs.inorgchem.9b00340
Inorg. Chem. 2019, 58, 7785−7793

cuvettes with a 1 cm path length. Infrared spectra were measured with a Nicolet 380 FT-IR spectrometer. $^1$H NMR spectra were obtained on a Varian 400 MR spectrometer (at 400 MHz) and are reported relative to $SiMe_4$ ($\delta$ 0.00) except the CsF titrations, which were reported relative to MeOH ($\delta$ 3.31). $^{13}$C NMR spectra were obtained on a Varian 400 MR spectrometer (at 100 MHz) and are reported relative to $SiMe_4$ ($\delta$ 0.00). NMR acquisition sequences for metal-containing species had a 1 ms relaxation delay, 90° pulse angle, and acquisition time of 1 s. EPR spectra were collected using a Bruker ESR-300 cooled under a flow of liquid $N_2$. EPR samples were prepared by dissolving the sample in MeOH (~0.05 M), transferring it to an NMR tube, and sealing the cap with parafilm. Elemental analyses were performed by Midwest Microlab, LLC in Indianapolis, IN.

**Mass Spectrometry Measurements.** Samples were prepared in a dinitrogen-filled glovebox by dissolving the metal complex in MeOH (to generate approximately 1 mM solutions of Fe complex) and sealing the vials with a cap. These solutions were transported to the spectrometer and were injected into the spectrometer as quickly as possible; brief exposure to air (~3 s) could not be avoided. Measurements were performed in the positive-ion mode on a Thermo LTQ mass spectrometer equipped with an analytical electrospray ion source and a quadrupole ion trap mass analyzer. Measurements were also performed in the negative-ion mode, but the results were not analyzed in detail due to low signal intensities. Unless otherwise noted, measurements were performed with capillary temperature = 175 °C, spray voltage = 5 kV, and spray current = 91 $\mu$A. All experiments were performed in MeOH, and the instrument was washed with 1 mL of solvent between scans. The peaks associated with Fe-containing complexes were identified, and their relative abundances were summed into categories defined by loss of 0, 1, 2, or 3 TBS groups (See Supporting Information, Tables S1–S4).

**Electrochemical Measurements.** Electrochemical experiments were performed in 0.1 M solutions of $Bu_4NPF_6$ in MeOH in a dinitrogen-filled glovebox. Cyclic voltammograms (CVs) and square-wave voltammograms (SWVs) were obtained with a CH Instruments potentiostat (model 1230A or 660C) using a 0.25 mm glassy carbon disk working electrode, $Ag^+$/Ag reference electrode and a Pt wire counter electrode. Scans were collected at rates between 0.10 V s$^{-1}$ and 10 V s$^{-1}$ for CVs and at a step-size of 0.004 V and a frequency of 15 Hz for SWVs. Reported potentials are referenced to the $[Cp_2Fe]^+$/$[Cp_2Fe]$ ($Fc^+$/Fc, where Cp = cyclopentadienyl) redox couple and were determined by adding ferrocenium tetrafluoroborate as an internal standard at the conclusion of each electrochemical experiment. Note that ferrocene could not be used as the internal standard as it is insoluble in MeOH.

**Magnetic Measurements.** Solid-state magnetic susceptibility data were collected for **4** using a Quantum Design MPMS XL SQUID magnetometer at temperatures between 2 and 300 K, and DC fields up to 20 kOe. In a dinitrogen-filled glovebox, powdered microcrystalline samples were loaded into polyethylene bags, sealed, and inserted into drinking straws for measurements. Ferromagnetic impurities were checked through a variable field measurement (0–20 kOe) of the magnetization at 100 K; curvature in the $M$ vs $H$ data obtained between 0 and 2 kOe (Figures S26 and S27) indicates the presence of minor ferromagnetic impurities. As a result, the magnetic susceptibility measurements were performed at a 5 kOe applied field, where the $M$ vs $H$ trace was linear. Data were corrected for the diamagnetic contributions of the sample holder and bag by subtracting empty containers; corrections for the sample were calculated from Pascal's constants.[42]

Evans' method determinations of magnetic susceptibility in solution for **2** and **4** were carried out using the residual protonated fraction of the indicated deuterated solvent in a capillary as a reference.[43] (Because of the presence of other silyl peaks in the $^1$H NMR spectra for **2** and **4**, $SiMe_4$ was not a reliable reference.) To obtain solution susceptibility data after the addition of CsF, different aliquots of a stock CsF solution (~0.3 M) in $CD_3OD$ were added to a solution of **2** or **4** (~0.01 M) in $CD_3OD$ in an NMR tube. The samples were then passed through a syringe filter to remove small amounts of colorless insoluble components. A capillary was then inserted, and the NMR tube was capped, sealed with parafilm, and quickly transported to a NMR spectrometer.

**Computational Methods.** For the computational study, the trimethylsilyl (TMS) substituent was used in place of TBS since the electronics are nearly identical, while the size of the calculation is reduced. The phenoxide substituent is the assumed product for the complete reaction of **2** with CsF. The singlet states of $[Fe(5\text{-}OTMSpy)_3tren]^{2+}$ and $[Fe(5\text{-}Opy)_3tren]^-$ (Figure 2) were optimized with the APFD functional[44] and the 6-311+g(d) basis set in the absence of counterions.[45,46]

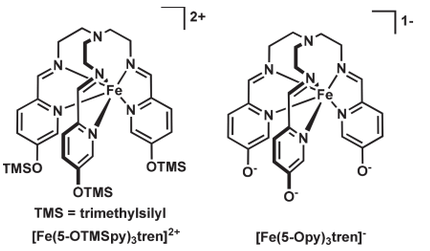


**Figure 2.** LS state geometry optimized model complexes of the desilylation reaction.

Calculations were performed with the PCM model[47] in an implicit solvent cavity of acetonitrile ($\varepsilon$ = 35.688). The APFD functional accurately reproduces the structural properties of the primary coordination sphere by comparison to analogous Fe(II) complexes.[48] Slight deviation between the structures is shown in the distances between the tertiary amine of the capping ligand and the Fe(II) center for the two structures, 3.40 and 3.45 Å for the silyl ether and phenoxide substituents, respectively. Since those distances exceed sums of the van der Waals radii, it is unlikely that the bridgehead nitrogen significantly impacts the ligand field properties of the complex within the current deviation.[49]

TD-DFT[50] was performed with the $\omega$B97XD functional[51] with settings identical to the optimization procedure. The functional was selected because of its treatment of charge transfer allows us to better probe the isolated ligand field states of the system. All DFT computations were performed with the Gaussian 16 software package.[52]

*Ab initio* ligand field theory (AILFT)[53,54] analyses were performed on the DFT-optimized structures through a CASSCF/NEVPT2 approach, using the ORCA 4.0 software package.[55] The AILFT treatment used a restricted active space consisting of the five 3d orbitals and with equal weighting of all possible states (5 singlets, 45 triplets, and 50 quintets for a d$^6$ system). The multireference computations were performed with the CPCM model[47] for acetonitrile and cc-pVDZ and cc-pVTZ[56] basis sets for the nonmetal atoms and Fe center, respectively. The solutions of the ligand field matrix and the transition states of the CASSCF and NEVPT2 output were each used to obtain a best fit of the $\sigma$- and $\pi$-bonding parameters of the angular overlap model (AOM), using the AOMX software.[57] $D_3$ symmetry was applied to the first coordination sphere polyhedra for $[Fe(5\text{-}OTMSpy)_3tren]^{2+}$ and $[Fe(5\text{-}Opy)_3tren]^-$ for the AOM parametrization.

## RESULTS AND DISCUSSION

**Syntheses and Characterizations of Fe Compounds.** The tripodal complexes **2** and **4** were prepared via Schiff-base condensation of the appropriate aldehyde (**1** or **3**, respectively) with tren, followed by addition of a ferrous salt to the in situ formed ligand (Scheme 1). The use of iron(II) perchlorate is crucial to obtain pure **4**, as attempts to obtain other salts in high purity (including triflate, chloride, bromide, tetraphenylborate, and tetrafluoroborate) were unsuccessful. Structural characterization of **2** was performed by single crystal X-ray


DOI: 10.1021/acs.inorgchem.9b00340
Inorg. Chem. 2019, 58, 7785–7793

**Scheme 1. Synthesis of Fe(II) Complexes 2 and 4**

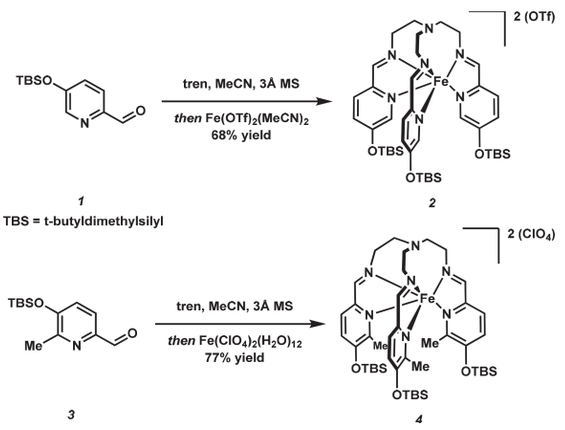


diffraction (Figure S25 and accompanying discussion in the Supporting Information), which confirmed the expected connectivity throughout the complex, yet contained severe disorder within the silyl groups, precluding a detailed analysis.

Room temperature (298 K) deuterated acetone solution magnetic susceptibility values for the Fe-containing compounds were acquired using Evans' method. For **2**, an obtained $\chi_M T$ value of 0.17 cm$^3$ K mol$^{-1}$ suggests a LS ground state, and thus solid-state magnetic susceptibility data were not collected. On the other hand, the 6-methylated species **4** exhibits a $\chi_M T$ value of 3.44 cm$^3$ K mol$^{-1}$, consistent with a HS Fe(II) species at room temperature, as expected.[8−10,12,13] The solid-state temperature dependence of $\chi_M T$ for **4** is shown in Figure 3.

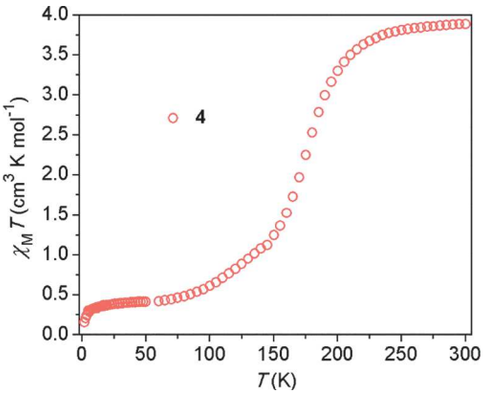


**Figure 3.** Temperature dependence of the magnetic susceptibility for **4** measured at an applied dc field of 5000 Oe.

At 300 K, the $\chi_M T$ value for **4** is 3.89 cm$^3$ K mol$^{-1}$, in agreement with a quintet state ($S$ = 2). Upon decreasing the temperature, the $\chi_M T$ product decreases slightly until ∼215 K, where the decrease becomes more pronounced, indicative of a spin crossover (SCO) event ($T_{1/2}$ = 175 K). This decrease continues until ∼120 K where the $\chi_M T$ product remains relatively constant at 0.40 cm$^3$ K mol$^{-1}$. The $T_{1/2}$ value and lower temperature magnetic susceptibility behavior are consistent with other 6-methylated 5-alkoxy Fe(II) trenpodand complexes that display SCO behavior in the solid state.[9,10] The $\chi_M T$ value does not reach 0 cm$^3$ K mol$^{-1}$ possibly due to a paramagnetic impurity that is not separable from **4**, which is fairly common for Fe(II) SCO materials;[28,58] alternatively, **4** might undergo incomplete SCO.

To assess the redox properties of **2** and **4**, their electrochemical properties were probed in methanol. The $E_{1/2}$ values for the Fe$^{III/II}$ couple of **2** and **4** are +0.95 and +0.97 V vs Fc$^+$/Fc, as obtained from SWV measurements (Figures S20 and S23), respectively. These values and overall behavior regarding reversibility compare well to previously characterized Fe(II) iminopyridine tripodal systems.[8,48,59] On the basis of cyclic voltammetry (CV) data, **2** displays a reversible Fe$^{III/II}$ couple at a scan rate of 0.10 V s$^{-1}$, while the analogous couple in **4** is apparently irreversible at the same scan rate (Figure 4). Upon increasing the scan rate to 10 V s$^{-1}$

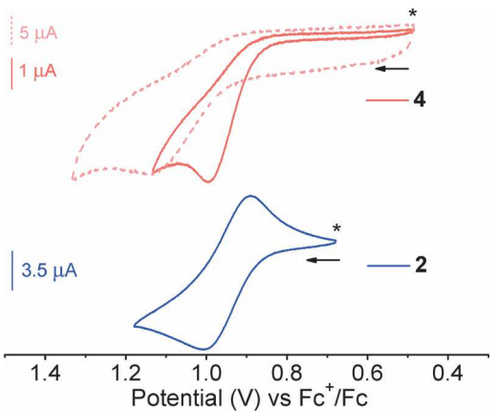


**Figure 4.** CVs of **2** (bottom) and **4** (top) measured in 0.10 M $Bu_4NPF_6$ solutions in MeOH, with scan rates of 0.10 V s$^{-1}$ (solid) or 10 V s$^{-1}$ (dashed). The asterisks indicate the open circuit potential, while the arrows indicate the direction of the scan, which in all cases is anodic.

(red dashed trace), the cyclic voltammogram (CV) shows an increase in current passed in the cathodic sweep, indicating that **4** does not exhibit completely irreversible behavior.

After the addition of excess CsF into the electrochemical cell containing **2**, the assigned Fe$^{III/II}$ redox event broadens and shifts cathodically by approximately 200 mV while still passing current in both the anodic and cathodic directions of scanning (Figure S21). This suggests that multiple desilylated species are formed and the shift in redox potential can be linked to a significant increase in negative charge on the ligand upon desilylation. Meanwhile, when excess CsF is added to **4**, a distinct redox event associated with the iron center is not observed at a scan rate of 0.1 V s$^{-1}$, although spectroscopic and ESI-MS data support the presence of Fe coordination complexes after CsF addition (vide infra). This supports the notion that solution stability upon desilylation is greater for LS **2** than HS **4**.

**In Situ Monitoring of Desilylation for 2 and 4.** Noting that compounds **2** and **4** are susceptible to decomposition in solution over time, we probed their solution stabilities and summarized the results in the Supporting Information; importantly, we found that the complexes remained intact over the time scale of all experiments included herein. In order to probe the effects of desilylation on Fe(II) spin state in **2** and **4**, additional techniques were employed. The results of in situ mass spectrometry and $^1$H NMR spectroscopy are presented in addition to the electrochemical experiments to provide a clearer picture of the desilylation reaction using CsF.

Importantly, we find that the identity of the fluoride source used is critical. We first tried tetrabutylammonium triphenyldi-



DOI: 10.1021/acs.inorgchem.9b00340
Inorg. Chem. 2019, 58, 7785−7793

fluorosilicate (TBAT), as it is readily soluble in polar aprotic solvents. Unfortunately, we found that addition of TBAT to solutions of **2** or **4** in MeCN induce immediate demetalation of the complexes, as evidenced by the appearance of free ligand peaks in the mass spectra (Figures S15 and S16), and a stark change in color from red to pale yellow (Figure S32). Alternative fluoride sources, including TBAF in tetrahydrofuran, KF/18-crown-6 in acetonitrile, and CsF/18-crown-6 in acetone, all show similar color changes. When CsF is used in methanol, however, mass spectrometry experiments indicate that the ligand was desilylated without significant demetalation. The results of the CsF titration experiments performed on **2** are presented in Figure 5.

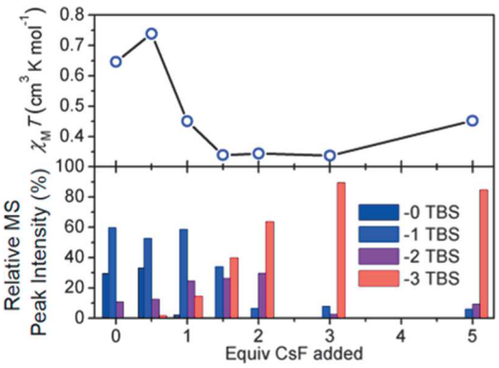


**Figure 5.** Top: solution state magnetic properties for **2** upon addition of CsF; the line is a guide to the eye. Bottom: relative abundance of Fe-containing desilylated ions for **2**, as determined by integrations of mass spectrometry intensities, relative to each individual spectrum. These data were collected in $CD_3OD$.

Here, we observe that the solution-phase $\chi_M T$ values decrease as CsF is titrated into the solution up to 1.5 equiv. We note the difference in $\chi_M T$ value at 0 equiv CsF added in $CD_3OD$ as compared to the value provided in $(CD_3)_2CO$, highlighting a difference in complex stability in these two solvents; see Supporting Information for further discussion (p S34). This is accompanied by an increase in relative abundance of peaks associated with desilylated complexes of Fe(II). These are detected as both protonated and nonprotonated species; for a full list of identity assignments in the positive ion mode, see Table S1. Overall low signal intensity in the negative ion mode precluded full interpretation of anions formed in the desilylation reactions; notwithstanding, $m/z$ values corresponding to triply desilylated species could be detected. Upon further addition of fluoride (up to 5 equiv), the magnetic susceptibility increases, while the trend of increased abundance of desilylated species continues as before. Noteworthy is that, at higher loadings of CsF during the mass spectrometry experiments, the overall intensity of the signals decreases, suggesting the formation of less ionizable products. In all, the combined NMR and MS experiments allow us to make a qualitative link between CsF addition and Fe complex desilylation, and that these species generally remain in a LS state over the course of the titration.

Similar effects are observed in the case of complex **4** (Figure 6). As before, addition of up to 1.5 equiv of fluoride leads to a decrease in magnetic susceptibility and the exclusive detection of ions identified as triply desilylated species in the ESI-MS. This suggests that fluoride-mediated cleavage may be super-

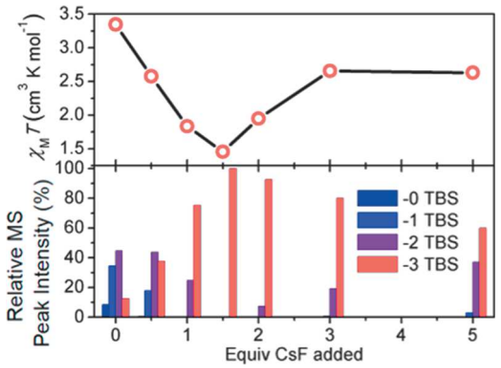


**Figure 6.** Top: solution-phase magnetic properties for **4** upon addition of CsF. Bottom: relative abundance of Fe-containing desilylated ions for **4**, as determined by integrations of mass spectrometry intensities, relative to each individual spectrum. These data were collected in $CD_3OD$.

stoichiometric. The complete desilylation that is observed for **4** (and not **2**) may be rationalized, given that HS complexes are often more reactive,[60,61] and the methyl groups proximal to the reaction site for **4** may contribute steric effects. Addition of further equivalents of fluoride leads to an increase in magnetic susceptibility and the disappearance of the signals corresponding to the fully silylated species. As was the case with **2**, there was also a reduction in the overall intensity of signal in the MS experiments.

An analysis of the NMR spectra of the desilylation reaction of **2** offers additional insight into the speciation in solution. First, there are several sets of pyridyl resonances present prior to addition of CsF and up until the addition of 5 equiv (Figures S39 and S40). This suggests there may be multiple species present in solution until a larger amount of CsF has been added to the sample. Once five equivalents are added, the spectrum indicates convergence to one major *C*3-symmetric species (Figure S39, bottom). Additionally, upon addition of CsF, the relative integration of the peaks associated with the pendant -OTBS moiety relative to the aromatic region decreases, indicating that this -TBS group is cleaved from the system. This analysis is more difficult to perform for paramagnetic **4** as the spectra are extended over a larger range ($\delta$ −14 to 173 ppm).

In conclusion, the experimental results presented indicate that for both **2** and **4** the titration of CsF leads to the formation of desilylated species. Further, these in situ formed Fe-complexes exhibit a decrease in overall magnetic susceptibility, which suggests that the spin-state equilibrium is shifted toward the LS state.

**Computational Results and Interpretation of Ligand Field Effects.** To further understand the observed spin-state changes, computations were performed on $[Fe(5\text{-}OTMSpy)_3tren]^{2+}$ and $[Fe(5\text{-}Opy)_3tren]^{-}$, models for **2** and its fully desilylated relative, respectively. We only consider the phenoxide substituents as the reaction product to probe the largest possible electronic impact in terms of Hammett parameter ($\sigma_{meta}$ = +0.09 → −0.47; $\sigma_{para}$ = +0.09 → −0.81). While the primary coordination sphere of the optimized structures ($Fe-N_{imine}$ and $Fe-N_{pyridine}$ distances and NNN torsion angle) is maintained, the desilylation alters the electronics of the ligand itself as shown in Figure 7. First, the C−O bond length of the substituent at the 5 position of the pyridine ring decreases by 0.07 Å upon desilylation. This


DOI: 10.1021/acs.inorgchem.9b00340
*Inorg. Chem.* 2019, 58, 7785−7793

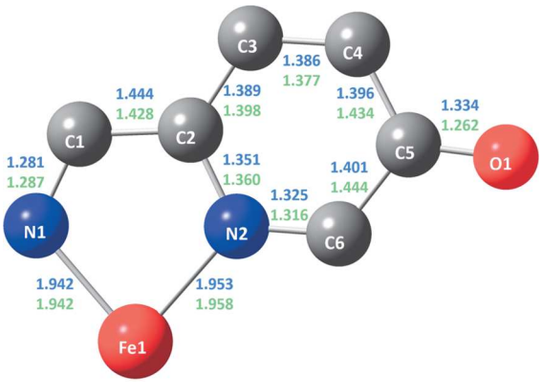


**Figure 7.** Optimized bond lengths (Å) of $[Fe(5\text{-}OTMSpy)_3tren]^{2+}$ (blue) and $[Fe(5\text{-}Opy)_3tren]^{-}$ (green) for the $C_3$ symmetric bidentate ligand. The hydrogen and remaining atoms of the tren-moiety are removed for clarity.

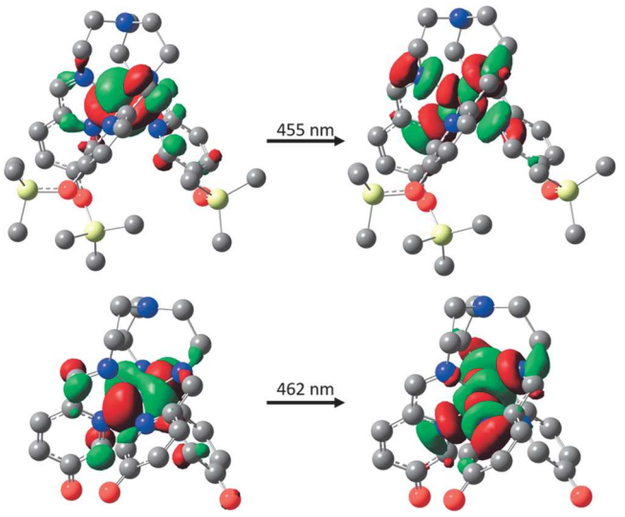


**Figure 8.** $\omega$B97XD/6-311+g(d) NTOs of $[Fe(5\text{-}OTMSpy)_3tren]^{2+}$ (top) and $[Fe(5\text{-}Opy)_3tren]^{-}$ (bottom) depicting the energy and orbital character associated with a $t_{2g} \rightarrow e_g^*$ excitation; hydrogen atoms are removed for clarity.

suggests that the desilylated functional group has significant carbonyl character, where the formal negative charge on the phenoxide is effectively delocalized into the aromatic system.

The electron-donating character of the phenoxide substituent displays competing impacts on the ligand field strength of the complex. The anionic charge is expected to increase the $\sigma$-donor ability of the coordinated nitrogen atoms through increased Lewis basicity. However, delocalization occurs through the conjugated system, which simultaneously decreases the $\pi^*$-acceptor ability of the diimine. Since the Hammett parameters combine inductive and resonance effects into a single variable, it is not sufficiently sophisticated to account for the $\sigma$- and $\pi$-electronic considerations of the substituent groups.[62]

TD-DFT was used to probe the d-orbital splitting through generation of low-energy electronic transitions of the model compounds. The long-range corrected (LC) $\omega$B97xd functional was selected because of its treatment of charge transfer interactions. Natural transition orbitals (NTOs)[63] of largely d-orbital character were obtained (Figure 8). These symmetry-forbidden ligand field excitations are obscured experimentally due to the broad and intense MLCT transitions of LS-Fe(II) compounds, as reported in the Supporting Information. The comparative energies exhibit a red-shift of 307 $cm^{-1}$ for the $t_{2g} \rightarrow e_g^*$ excitation (Figure 8, labels assume local octahedral symmetry), which suggests the phenoxide substituent weakens the ligand field strength through dominant $\pi$-effects. This agrees with previous experimental results on Fe(II) ligand sets with *para*-substituted pyridine groups.[18,32,64,65]

We also considered the impact of the overall charge as well as increased hydrogen bond-accepting ability of the phenoxide substituent on the ligand field transitions. Additional TD-DFT calculations were performed on $[Fe(5\text{-}Opy)_3tren]^{-}$ where a phenoxide group was docked with (a) solvent methanol molecule in a hydrogen-bonding orientation, and (b) a sodium cation in a close ion pair. Coordinates and TD-DFT results of the structures are included in Tables S12–S13. In both instances, the ligand field transition maintained a value of 462 nm for the iron-containing moiety $[Fe(5\text{-}Opy)_3tren]^{-}$. These results suggest the differences of charge and hydrogen-bonding ability do not impact ligand field strength.

To gain further insight into the character of the d–d transitions, *ab initio* ligand field theory (AILFT) was used. This has previously been successful in the treatment of Fe(II) complexes[66–68] through a CASSCF/NEVPT2 d-orbital active space, which treats all the available ligand field excitations of the metal center. The d-orbital energies obtained by AILFT corroborate the TD-DFT results, with the magnitude of the d-orbital splitting decreasing only slightly upon desilylation. The ligand field splitting for $[Fe(5\text{-}OTMSpy)_3tren]^{2+}$ is 20360 $cm^{-1}$ and decreases to 20 195 $cm^{-1}$ for $[Fe(5\text{-}Opy)_3tren]^{-}$.

The AILFT excitation energies were parametrized with the angular overlap model (AOM) to quantify the fluctuations in $\sigma$- and $\pi$-bonding, $e_\sigma$ and $e_\pi$, due to substituent identity. The differences in these values obtained at the NEVPT2 and CASSCF levels of theory have been previously correlated with the covalency of the metal–ligand interaction.[69] The $e_\sigma$(NEVPT2-CASSCF) increases by 115 $cm^{-1}$, while $e_\pi$(NEVPT2-CASSCF) increases by 100 $cm^{-1}$, weakening the bonding character of the $t_{2g}$ orbitals through desilylation. Since the $\sigma$- and $\pi$-effects are of comparable magnitude (for reference, $\Delta = 3e_\sigma - 4e_\pi$, for complexes with $O_h$ symmetry), only a minute change is imparted on the overall ligand field strength, despite the significant change in the electron-donating character of the substituent group. In total, we find no large dependence of substituent identity on the electronic structure of the complex, regardless of the level-of-theory applied.

We note that a strictly electronic analysis only accounts for enthalpic contributions of ligand field strength and does not consider entropic impacts of substituent identity. While the electronic calculations suggest a preference for the HS state upon desilylation, the in situ Evans' method data show a decrease in solution-phase $\chi_M T$ values upon addition of fluoride. Although our calculations indicate that the silyl ether group provides a stronger ligand field, it also has vibrational degrees of freedom (3N-6, where N is the number of atoms) which are not present with respect to the phenoxide group. The stark contrast in the degrees of freedom of these substituent groups may provide a simultaneous probe for fluctuations in $\Delta S$ between the complexes.

The trigonal-pocket formed by the presence of the substituents at the 5-position of the tren-iminopyridine scaffold


DOI: 10.1021/acs.inorgchem.9b00340
*Inorg. Chem.* 2019, 58, 7785–7793

offers close contacts between the -OTMS groups in the optimized structure (Figure 9). These van der Waals contacts

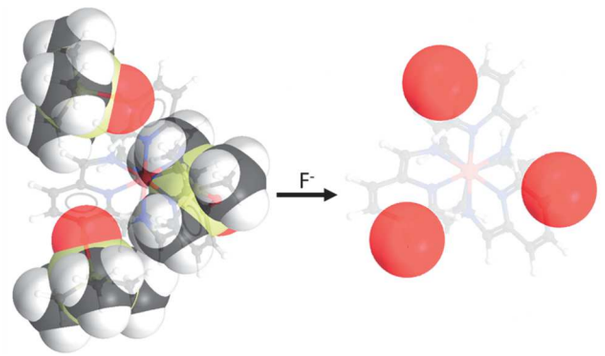


**Figure 9.** $[Fe(5\text{-}OTMSpy)_3tren]^{2+}$ (left) and $[Fe(5\text{-}Opy)_3tren]^{-}$ (right) oriented along the $C_3$-axis in which the 5-substituents are modeled with respect to their van der Waals radii.

hinder the conformational freedom of the silyl ether groups; such steric hindrance can be alleviated through the volume expansion of the complex associated with the increased bond lengths in the HS state. In addition, the silyl ether-containing compound possesses more low-frequency vibrational modes than the desilylated compound. This is anticipated to significantly contribute to the overall entropy change upon SCO. Overall, the loss of these vibrational modes and reduced steric crowding upon desilylation is expected to shift the equilibrium to the LS state, as is observed in the decreasing magnetic susceptibility. We note that a favored HS state has previously been attributed to the conformational disorder associated with the *n*-alkyl substituents of analogous Fe(II) complexes.[9,70,71]

## CONCLUSIONS

This study sheds light on the structural and electronic impacts of postsynthetic modifications of Fe(II) complexes containing a silylated ligand scaffold. Specifically, the feasibility of performing a desilylation reaction to impart a spin-state change on an Fe(II) center is probed. Our results indicate that desilylation of **2** and **4** promotes a shift toward a lower overall spin-state in both cases. For these complexes, the computational results suggest that changes in substituent identity do not appreciably alter ligand field strength, implicating entropic perturbations as the probable source for the observed spin-state changes. These considerations suggest an alternative approach to the design of SCO compounds, where release of steric strain through substituent change may drive spin-state switching. In the future, we envision that similar desilylation processes applied on closely related Fe(II) analogs with slightly weaker ligand fields may find utility in fluoride sensing applications, as the LS species **2** has significantly stronger absorption in the visible spectrum than the HS counterpart **4**.

## ASSOCIATED CONTENT

### Supporting Information

The Supporting Information is available free of charge on the ACS Publications website at DOI: 10.1021/acs.inorgchem.9b00340.

Ligand synthesis; ESI-MS spectra and characterization; electrochemical, NMR, UV−vis, and magnetic analyses; discussion of solution stability of **2** and **4**; Cartesian coordinates and NTOs from output of DFT optimizations; ligand field splitting and AOM parameters from *ab initio* output (PDF)

### Accession Codes

CCDC 1816444 contains the supplementary crystallographic data for this paper. These data can be obtained free of charge via www.ccdc.cam.ac.uk/data_request/cif, or by emailing data_request@ccdc.cam.ac.uk, or by contacting The Cambridge Crystallographic Data Centre, 12 Union Road, Cambridge CB2 1EZ, UK; fax: +44 1223 336033.

## AUTHOR INFORMATION


### Corresponding Author

*E-mail: matthew.shores@colostate.edu.

### ORCID

Tarik J. Ozumerzifon: 0000-0001-7568-4679
Robert F. Higgins: 0000-0001-6776-3537
Justin P. Joyce: 0000-0002-8287-622X
Jacek L. Kolanowski: 0000-0002-6779-4736
Anthony K. Rappé: 0000-0002-5259-1186
Matthew P. Shores: 0000-0002-9751-0490

### Present Addresses

[#](T.J.O.) Isola Group, Chandler, AZ 85224, United States.
[∥](R.F.H.) P. Roy and Diana T. Vagelos Laboratories, Department of Chemistry, University of Pennsylvania, Philadelphia, Pennsylvania 19104, United States.


### Notes

The authors declare no competing financial interest.

## ACKNOWLEDGMENTS

This work is supported by Colorado State University and the NSF (CHE-1363274 and CHE-1800554). J.L.K. acknowledges funding from the Polish Ministry of Science and Higher Education (the KNOW program). We thank Dr. Mihail Atanasov of the Max Planck Institut für Kohlenforschung for providing the AOMX software. We also thank the Central Instrument Facility at Colorado State University for assistance with mass spectrometry analysis.

## REFERENCES

(1) Gütlich, P.; Hauser, A.; Spiering, H. Thermal and Optical Switching of Iron(II) Complexes. *Angew. Chem., Int. Ed. Engl.* **1994**, *33*, 2024−2054.
(2) Gütlich, P.; Garcia, Y.; Goodwin, H. A. Spin crossover phenomena in Fe(II) complexes. *Chem. Soc. Rev.* **2000**, *29*, 419−427.
(3) Halcrow, M. A. The spin-states and spin-transitions of mononuclear iron(II) complexes of nitrogen-donor ligands. *Polyhedron* **2007**, *26*, 3523−3576.
(4) Cook, L. J. K.; Mohammed, R.; Sherborne, G.; Roberts, T. D.; Alvarez, S.; Halcrow, M. A. Spin state behavior of iron(II)/dipyrazolylpyridine complexes. New insights from crystallographic and solution measurements. *Coord. Chem. Rev.* **2015**, *289−290*, 2−12.
(5) Hogue, R. W.; Singh, S.; Brooker, S. Spin crossover in discrete polynuclear iron(II) complexes. *Chem. Soc. Rev.* **2018**, *47*, 7303−7338.
(6) Khusniyarov, M. M. How to Switch Spin-Crossover Metal Complexes at Constant Room Temperature. *Chem. - Eur. J.* **2016**, *22*, 15178−15191.
(7) Ashley, D. C.; Jakubikova, E. Ironing out the photochemical and spin-crossover behavior of Fe(II) coordination compounds with computational chemistry. *Coord. Chem. Rev.* **2017**, *337*, 97−111.


DOI: 10.1021/acs.inorgchem.9b00340
*Inorg. Chem.* 2019, 58, 7785−7793

(8) Hoselton, M. A.; Wilson, L. J.; Drago, R. S. Substituent Effects on Spin Equilibrium Observed with Hexadentate Ligands on Iron(II). *J. Am. Chem. Soc.* **1975**, *97*, 1722−1729.
(9) Seredyuk, M.; Gaspar, A. B.; Ksenofontov, V.; Galyametdinov, Y.; Kusz, J.; Gütlich, P. Does the solid-liquid crystal phase transition provoke the spin-state change in spin-crossover metallomesogens? *J. Am. Chem. Soc.* **2008**, *130*, 1431−1439.
(10) Seredyuk, M.; Munoz, M. C.; Ksenofontov, V.; Gütlich, P.; Galyametdinov, Y.; Real, J. A. Spin Crossover Star-Shaped Metallomesogens of Iron(II). *Inorg. Chem.* **2014**, *53*, 8442−8454.
(11) Fatur, S. M.; Shepard, S. G.; Higgins, R. F.; Shores, M. P.; Damrauer, N. H. A Synthetically Tunable System To Control MLCT Excited-State Lifetimes and Spin States in Iron(II) Polypyridines. *J. Am. Chem. Soc.* **2017**, *139*, 4493−4505.
(12) Schultz, D.; Nitschke, J. R. Choices of iron and copper: Cooperative selection during self-assembly. *Angew. Chem., Int. Ed.* **2006**, *45*, 2453−2456.
(13) Schenker, S.; Hauser, A.; Wang, W.; Chan, I. Y. High-spin -> low-spin relaxation in $[Zn_{1-x}Fex(6\text{-mepy})_{3-y}(py)_y$ tren$](PF6)_2$. *J. Chem. Phys.* **1998**, *109*, 9870−9878.
(14) Miller, T.; Holloway, L. R.; Nye, P. P.; Lyon, Y.; Beran, J. O.; Harman, W. H.; Julian, J. R.; Hooley, R. J. Small Structural Variations Have Large Effects on the Assembly Properties and Spin State of Room Temperature High Spin Fe(II) Iminopyridine Cages. *Inorg. Chem.* **2018**, *57*, 13386−13396.
(15) Kolanowski, J. L.; Jeanneau, E.; Steinhoff, R.; Hasserodt, J. Bispidine Platform Grants Full Control over Magnetic State of Ferrous Chelates in Water. *Chem. - Eur. J.* **2013**, *19*, 8839−8849.
(16) Ni, Z. P.; Shores, M. P. Magnetic Observation of Anion Binding in Iron Coordination Complexes: Toward Spin-Switching Chemosensors. *J. Am. Chem. Soc.* **2009**, *131*, 32−33.
(17) Sahoo, D.; Quesne, M. G.; De Visser, S. P.; Rath, S. P. Hydrogen-Bonding Interactions Trigger a Spin-Flip in Iron(III) Porphyrin Complexes. *Angew. Chem., Int. Ed.* **2015**, *54*, 4796−4800.
(18) Cook, L. J. K.; Kulmaczewski, R.; Mohammed, R.; Dudley, S.; Barrett, S. A.; Little, M. A.; Deeth, R. J.; Halcrow, M. A. A Unified Treatment of the Relationship Between Ligand Substituents and Spin State in a Family of Iron(II) Complexes. *Angew. Chem., Int. Ed.* **2016**, *55*, 4327−4331.
(19) Rodríguez-Jiménez, S.; Yang, M. R.; Stewart, I.; Garden, A. L.; Brooker, S. A Simple Method of Predicting Spin State in Solution. *J. Am. Chem. Soc.* **2017**, *139*, 18392−18396.
(20) Kimura, A.; Ishida, T. Spin-Crossover Temperature Predictable from DFT Calculation for Iron(II) Complexes with 4-Substituted Pybox and Related Heteroaromatic Ligands. *ACS Omega.* **2018**, *3*, 6737−6747.
(21) Park, J. G.; Jeon, I.-R.; Harris, T. D. Electronic Effects of Ligand Substitution on Spin Crossover in a Series of Diiminoquinonoid-Bridged $Fe^{II}_2$ Complexes. *Inorg. Chem.* **2015**, *54*, 359−369.
(22) Ashley, D. C.; Jakubikova, E. Tuning the Redox Potentials and Ligand Field Strength of Fe(II) Polypyridines: The Dual p-Donor and p-Acceptor Character of Bipyridine. *Inorg. Chem.* **2018**, *57*, 9907−9917.
(23) Lètard, J. F.; Guionneau, P.; Goux-Capes, L. Towards spin crossover applications. *Top. Curr. Chem.* **2004**, *235*, 221−249.
(24) Halcrow, M. A. *Spin-Crossover Materials: Properties and Applications*; John Wiley & Sons: West Sussex, UK, 2013.
(25) Gütlich, P.; Gaspar, A. B.; Garcia, Y. Spin state switching in iron coordination compounds. *Beilstein J. Org. Chem.* **2013**, *9*, 342−391.
(26) Touti, F.; Maurin, P.; Hasserodt, J. Magnetogenesis under Physiological Conditions with Probes that Report on (Bio-)Chemical Stimuli. *Angew. Chem., Int. Ed.* **2013**, *52*, 4654−4658.
(27) Gondrand, C.; Touti, F.; Godart, E.; Berezhanskyy, Y.; Jeanneau, E.; Maurin, P.; Hasserodt, J. Spring-Loaded Iron(II) Complexes as Magnetogenic Probes Reporting on a Chemical Analyte in Water. *Eur. J. Inorg. Chem.* **2015**, *2015*, 1376−1382.
(28) Milek, M.; Heinemann, F. W.; Khusniyarov, M. M. Spin Crossover Meets Diarylethenes: Efficient Photoswitching of Magnetic Properties in Solution at Room Temperature. *Inorg. Chem.* **2013**, *52*, 11585−11592.
(29) Rösner, B.; Milek, M.; Witt, A.; Gobaut, B.; Torelli, P.; Fink, R. H.; Khusniyarov, M. M. Reversible Photoswitching of a Spin-Crossover Molecular Complex in the Solid State at Room Temperature. *Angew. Chem., Int. Ed.* **2015**, *54*, 12976−12980.
(30) Nihei, M.; Suzuki, Y.; Kimura, N.; Kera, Y.; Oshio, H. Bidirectional Photomagnetic Conversions in a Spin-Crossover Complex with a Diarylethene Moiety. *Chem. - Eur. J.* **2013**, *19*, 6946−6949.
(31) Clements, J. E.; Price, J. R.; Neville, S. M.; Kepert, C. J. Perturbation of Spin Crossover Behavior by Covalent Post-Synthetic Modification of a Porous Metal-Organic Framework. *Angew. Chem., Int. Ed.* **2014**, *53*, 10164−10168.
(32) Gaudette, A. I.; Thorarinsdottir, A. E.; Harris, T. D. pH-Dependent spin state population and $^{19}F$ NMR chemical shift via remote ligand protonation in an iron(II) complex. *Chem. Commun.* **2017**, *53*, 12962−12965.
(33) Hasserodt, J.; Kolanowski, J. L.; Touti, F. Magnetogenesis in Water Induced by a Chemical Analyte. *Angew. Chem., Int. Ed.* **2014**, *53*, 60−73.
(34) Holloway, L. R.; Bogie, P. M.; Lyon, Y.; Julian, R. R.; Hooley, R. J. Stereoselective Postassembly CH Oxidation of Self-Assembled Metal-Ligand Cage Complexes. *Inorg. Chem.* **2017**, *56*, 11435−11442.
(35) Young, M. C.; Johnson, A. M.; Hooley, R. J. Self-promoted post-synthetic modification of metal-ligand $M_2L_3$ mesocates. *Chem. Commun.* **2014**, *50*, 1378−1380.
(36) Roberts, D. A.; Castilla, A. M.; Ronson, T. K.; Nitschke, J. R. Post-assembly Modification of Kinetically Metastable $Fe^{II}_2L_3$ Triple Helicates. *J. Am. Chem. Soc.* **2014**, *136*, 8201−8204.
(37) Roberts, D. A.; Pilgrim, B. S.; Cooper, J. D.; Ronson, T. K.; Zarra, S.; Nitschke, J. R. Post-assembly Modification of Tetrazine-Edged $Fe^{II}_4L_6$ Tetrahedra. *J. Am. Chem. Soc.* **2015**, *137*, 10068−10071.
(38) McConnell, A. J.; Aitchison, C. M.; Grommet, A. B.; Nitschke, J. R. Subcomponent Exchange Transforms an $Fe^{II}_4L_4$ Cage from High- to Low-Spin, Switching Guest Release in a Two-Cage System. *J. Am. Chem. Soc.* **2017**, *139*, 6294−6297.
(39) Klug, C. M.; McDaniel, A. M.; Fiedler, S. R.; Schulte, K. A.; Newell, B. S.; Shores, M. P. Anion dependence in the spin-crossover properties of a Fe(II) podand complex. *Dalton Trans.* **2012**, *41*, 12577−12585.
(40) McDaniel, A. M.; Klug, C. M.; Shores, M. P. Synthesis of Functionalized Hexadentate Iminopyridine Fe-II Complexes - Toward Anion-Dependent Spin Switching in Polar Media. *Eur. J. Inorg. Chem.* **2013**, *2013*, 943−950.
(41) Hansch, C.; Leo, A.; Taft, R. W. A Survey of Hammett Substituent Constants and Resonance and Field Parameters. *Chem. Rev.* **1991**, *91*, 165−195.
(42) Bain, G. A.; Berry, J. F. Diamagnetic corrections and Pascal's constants. *J. Chem. Educ.* **2008**, *85*, 532−536.
(43) Evans, D. F. The Determination of the Paramagnetic Susceptibility of Substances in Solution by Nuclear Magnetic Resonance. *J. Chem. Soc.* **1959**, *0*, 2003−2005.
(44) Austin, A.; Petersson, G. A.; Frisch, M. J.; Dobek, F. J.; Scalmani, G.; Throssell, K. A Density Functional with Spherical Atom Dispersion Terms. *J. Chem. Theory Comput.* **2012**, *8*, 4989−5007.
(45) Krishnan, R.; Binkley, J. S.; Seeger, R.; Pople, J. A. Self-Consistent Molecular-Orbital Methods. XX. Basis Set for Correlated Wave-Functions. *J. Chem. Phys.* **1980**, *72*, 650−654.
(46) Hay, P. J. Gaussian Basis Sets for Molecular Calculations - Representation of 3d Orbitals in Transition-Metal Atoms. *J. Chem. Phys.* **1977**, *66*, 4377−4384.
(47) Tomasi, J.; Mennucci, B.; Cammi, R. Quantum mechanical continuum solvation models. *Chem. Rev.* **2005**, *105*, 2999−3093.
(48) McDaniel, A. M.; Rappé, A. K.; Shores, M. P. Structural and Electronic Comparison of 1st Row Transition Metal Complexes of a Tripodal Iminopyridine Ligand. *Inorg. Chem.* **2012**, *51*, 12493−12502.


DOI: 10.1021/acs.inorgchem.9b00340
*Inorg. Chem.* 2019, 58, 7785−7793

(49) Halcrow, M. A. Structure:function relationships in molecular spin-crossover complexes. *Chem. Soc. Rev.* **2011**, *40*, 4119−4142.
(50) Stratmann, R. E.; Scuseria, G. E.; Frisch, M. J. An efficient implementation of time-dependent density-functional theory for the calculation of excitation energies of large molecules. *J. Chem. Phys.* **1998**, *109*, 8218−8224.
(51) Chai, J. D.; Head-Gordon, M. Long-range corrected hybrid density functionals with damped atom-atom dispersion corrections. *Phys. Chem. Chem. Phys.* **2008**, *10*, 6615−6620.
(52) Frisch, M. J. T., Trucks, G. W.; Schlegel, H. B.; Scuseria, G. E.; Robb, M. A.; Cheeseman, J. R.; Scalmani, G.; Barone, V.; Petersson, G. A.; Nakatsuji, H.; Li, X.; Caricato, M.; Marenich, A. V.; Bloino, J.; Janesko, B. G.; Gomperts, R.; Mennucci, B.; Hratchian, H. P.; Ortiz, J. V.; Izmaylov, A. F.; Sonnenberg, J. L.; Williams-Young, D.; Ding, F.; Lipparini, F.; Egidi, F.; Goings, J.; Peng, B.; Petrone, A.; Henderson, T.; Ranasinghe, D.; Zakrzewski, V. G.; Gao, J.; Rega, N.; Zheng, G.; Liang, W.; Hada, M.; Ehara, M.; Toyota, K.; Fukuda, R.; Hasegawa, J.; Ishida, M.; Nakajima, T.; Honda, Y.; Kitao, O.; Nakai, H.; Vreven, T.; Throssell, K.; Montgomery, J. A., Jr.; Peralta, J. E.; Ogliaro, F.; Bearpark, M. J.; Heyd, J. J.; Brothers, E. N.; Kudin, K. N.; Staroverov, V. N.; Keith, T. A.; Kobayashi, R.; Normand, J.; Raghavachari, K.; Rendell, A. P.; Burant, J. C.; Iyengar, S. S.; Tomasi, J.; Cossi, M.; Millam, J. M.; Klene, M.; Adamo, C.; Cammi, R.; Ochterski, J. W.; Martin, R. L.; Morokuma, K.; Farkas, O.; Foresman, J. B.; Fox, D. J. *Gaussian 16*, Revision B.01; Gaussian, Inc.: Wallingford, CT, 2016.
(53) Atanasov, M.; Zadrozny, J. M.; Long, J. R.; Neese, F. A theoretical analysis of chemical bonding, vibronic coupling, and magnetic anisotropy in linear iron(II) complexes with single-molecule magnet behavior. *Chem. Sci.* **2013**, *4*, 139−156.
(54) Van Stappen, C.; Maganas, D.; DeBeer, S.; Bill, E.; Neese, F. Investigations of the Magnetic and Spectroscopic Properties of V(III) and V(IV) Complexes. *Inorg. Chem.* **2018**, *57*, 6421−6438.
(55) Neese, F. Software update: the ORCA program system, version 4.0. *Wires Comput. Mol. Sci.* **2018**, *8*, No. e1327.
(56) Dunning, T. H. Gaussian-Basis Sets for Use in Correlated Molecular Calculations. I. The Atoms Boron through Neon and Hydrogen. *J. Chem. Phys.* **1989**, *90*, 1007−1023.
(57) Adamsky, H.; Schönherr, T.; Atanasov, M. AOMX: angular overlap model computation. *Comp. Coordin. Chem. II* **2003**, *2*, 661−664.
(58) Van der Meer, M.; Rechkemmer, Y.; Breitgoff, F. D.; Dechert, S.; Marx, R.; Dorfel, M.; Neugebauer, P.; Van Slageren, J.; Sarkar, B. Probing bistability in Fe(II) and Co(II) complexes with an unsymmetrically substituted quinonoid ligand. *Dalton Trans.* **2016**, *45*, 8394−8403.
(59) Larsen, E.; Lamar, G. N.; Wagner, B. E.; Holm, R. H.; Parks, J. E. 3-Dimensional Macrocyclic Encapsulation Reactionss.III. Geometrical Anelectronic Features of Tris(Diimine) Complexes of Trigonal-Prismatic, Antiprismatic, and Intermediate Stereochemistry. *Inorg. Chem.* **1972**, *11*, 2652−2668.
(60) Holland, P. L. Electronic structure and reactivity of three-coordinate iron complexes. *Acc. Chem. Res.* **2008**, *41*, 905−914.
(61) Chirik, P. J. Carbon-Carbon Bond Formation in a Weak Ligand Field: Leveraging Open-Shell First-Row Transition-Metal Catalysts. *Angew. Chem., Int. Ed.* **2017**, *56*, 5170−5181.
(62) Krygowski, T. M.; Stępień, B. T. s- and p-electron delocalization: Focus on substituent effects. *Chem. Rev.* **2005**, *105*, 3482−3512.
(63) Martin, R. L. Natural transition orbitals. *J. Chem. Phys.* **2003**, *118*, 4775−4777.
(64) Prat, I.; Company, A.; Corona, T.; Parella, T.; Ribas, X.; Costas, M. Assessing the Impact of Electronic and Steric Tuning of the Ligand in the Spin State and Catalytic Oxidation Ability of the $Fe^{II}$(Pytacn) Family of Complexes. *Inorg. Chem.* **2013**, *52*, 9229−9244.
(65) Nakano, K.; Suemura, N.; Yoneda, K.; Kawata, S.; Kaizaki, S. Substituent effect of the coordinated pyridine in a series of pyrazolato bridged dinuclear diiron(II) complexes on the spin-crossover behavior. *Dalton Trans.* **2005**, 740−743.
(66) Chilkuri, V. G.; DeBeer, S.; Neese, F. Revisiting the Electronic Structure of FeS Monomers Using ab Initio Ligand Field Theory and the Angular Overlap Model. *Inorg. Chem.* **2017**, *56*, 10418−10436.
(67) Atanasov, M.; Ganyushin, D.; Pantazis, D. A.; Sivalingam, K.; Neese, F. Detailed Ab Initio First-Principles Study of the Magnetic Anisotropy in a Family of Trigonal Pyramidal Iron(II) Pyrrolide Complexes. *Inorg. Chem.* **2011**, *50*, 7460−7477.
(68) Deeth, R. J.; Halcrow, M. A.; Cook, L. J. K.; Raithby, P. R. Ab Initio Ligand Field Molecular Mechanics and the Nature of Metal-Ligand p-Bonding in Fe(II) 2,6-di(pyrazol-1-yl)pyridine Spin Crossover Complexes. *Chem. - Eur. J.* **2018**, *24*, 5204−5212.
(69) Singh, S. K.; Eng, J.; Atanasov, M.; Neese, F. Covalency and chemical bonding in transition metal complexes: An ab initio based ligand field perspective. *Coord. Chem. Rev.* **2017**, *344*, 2−25.
(70) Delgado, T.; Tissot, A.; Guénée, L.; Hauser, A.; Valverde-Muñoz, F. J.; Seredyuk, M.; Real, J. A.; Pillet, S.; Bendeif, E. E.; Besnard, C. Very Long-Lived Photogenerated High-Spin Phase of a Multistable Spin-Crossover Molecular Material. *J. Am. Chem. Soc.* **2018**, *140*, 12870−12876.
(71) Galadzhun, I.; Kulmaczewski, R.; Cespedes, O.; Yamada, M.; Yoshinari, N.; Konno, T.; Halcrow, M. A. 2,6-Bis(pyrazol-1-yl)pyridine-4-carboxylate Esters with Alkyl Chain Substituents and Their Iron(II) Complexes. *Inorg. Chem.* **2018**, *57*, 13761−13771.


DOI: 10.1021/acs.inorgchem.9b00340
*Inorg. Chem.* 2019, 58, 7785−7793